Construction of a Near-Infrared-Activatable Enzyme Platform To Remotely Trigger Intracellular Signal Transduction Using an Upconversion Nanoparticle

Hua-De Gao,[†] Pounraj Thanasekaran,[†] Chao-Wei Chiang,[†] Jia-Lin Hong,[†] Yen-Chun Liu,[‡] Yu-Hsu Chang,[‡] and Hsien-Ming Lee*[,†]

[†]Institute of Chemistry, Academia Sinica, 128 Academia Road, Section 2, Nankang, Taipei 11529, Taiwan and [‡]Department of Materials and Mineral Resources Engineering, National Taipei University of Technology, 1 Zhongxiao E. Road, Section 3, Taipei 10608, Taiwan

ABSTRACT Photoactivatable (caged) bioeffectors provide a way to remotely trigger or disable biochemical pathways in living organisms at a desired time and location with a pulse of light (uncaging), but the phototoxicity of ultraviolet (UV) often limits its application. In this study, we have demonstrated the near-infrared (NIR) photoactivatable enzyme platform using protein kinase A (PKA), an important enzyme in cell biology. We successfully photoactivated PKA using NIR to phosphorylate its substrate, and this induced a downstream cellular response in living cells with high spatiotemporal resolution. In addition, this system allows NIR to selectively activate the caged enzyme immobilized on the nanoparticle surface without activating other caged proteins in the cytosol. This NIR-responsive enzyme—nanoparticle system provides an innovative approach to remote-control proteins and enzymes, which can be used by researchers who need to avoid direct UV irradiation or use UV as a secondary channel to turn on a bioeffector.

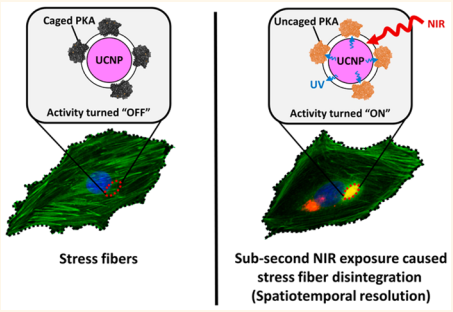

KEYWORDS: cellular activity · enzyme · photoactivation · proteins · upconversion nanoparticles

Photocaged proteins and enzymes generated *via* chemical modification, with the help of microinjection, are powerful tools to study intracellular signal transduction pathways.[1−19] Microinjecting chemically modified protein into cells is the most direct and quantitative approach to deliver protein into the cytosol, where important signal transduction occurs. It has fewer problems with endosomal entrapment or lysosomal degradation of the caged protein-of-interest, so it is commonly used in signal transduction studies.[7,20−23] Ultraviolet A (UVA 315−400 nm) irradiation provides excellent spatial and temporal control in activating the caged protein.[24−27] However, UVA exposure also triggers undesired signal transduction pathways, such as morphological changes, carcinogenesis, and apoptosis, due to photodamage of proteins, lipids, and nucleic acids.[9−19] Hence, many efforts has been devoted to two-photon irradiation[28−30] or longer wavelength[31] responsive caging groups, the latter of which provides more choices in uncaging wavelengths (channels) and selective activation for complex experiments with two or more bioeffectors.[7,31] Here, we report the near-infrared (NIR)-induced protein/enzyme activation system composed of chemically modified protein complexed with a lanthanide-doped upconversion nanoparticle (UCNP). This methodology not only avoids the undesired cellular response from direct UV irradiation, but also provides a wavelength-distinct activation channel when more than one cage-effector needs to be selectively turned on.

Upconversion nanoparticles (UCNPs), such as sodium yttrium fluoride ($NaYF_4$) nanocrystals codoped with Yb^{3+} (as a sensitizer) and Er^{3+}, Ho^{3+}, Tm^{3+} (as emitters), can generate highly efficient anti-Stokes luminescence.

* Address correspondence to leehm@chem.sinica.edu.tw.

Received for review March 12, 2015 and accepted June 23, 2015.

Published online June 23, 2015
10.1021/acsnano.5b01573

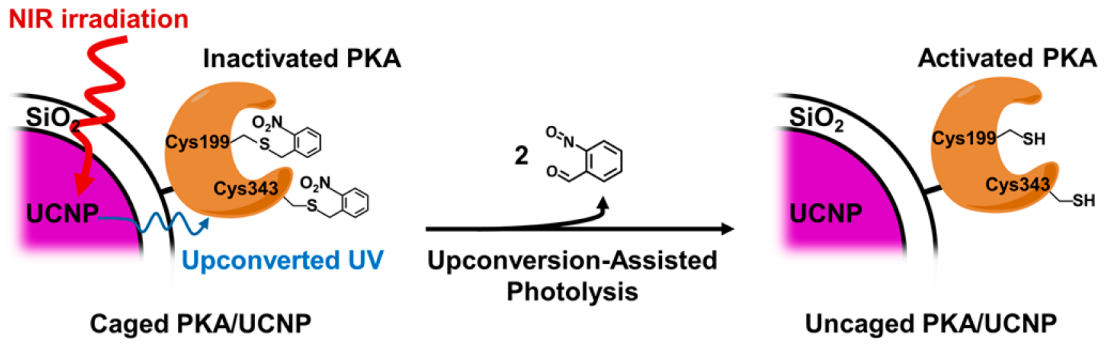

Scheme 1. Caged PKA/UCNP Complex Design and the Process of Upconversion-Assisted PKA Uncaging

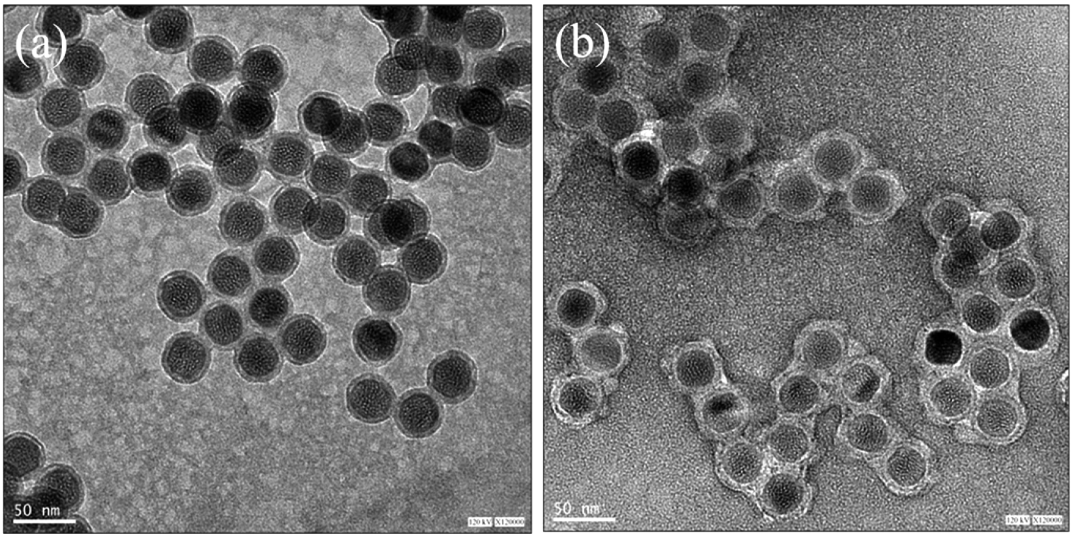

Figure 1. TEM images of (a) silica-coated UCNP, and (b) caged PKA immobilized on the surface of silica-coated UCNP. Samples were negatively stained with 2% uranyl acetate. Scale bar: 50 μm in all images.

They are effective transducers that convert the NIR excitation light to UV near the particle surface. Hence, UCNPs have received significant attention for applications in long-wavelength photolysis.[32,33] This developed material has been used to photoactivate small molecules, such as luminophore,[33,34] folic acid,[35] cisplatin derivatives,[36,37] DNA/siRNA,[38,39] and to trigger controlled-release systems, such as porous silica,[32,40,41] copolymer vesicles,[42,43] and hollow particles.[44,45] These studies laid important ground for UCNP-assisted photoactivation techniques. Surprisingly, there are no examples of such approaches for the activation of enzymes, which are an extremely important class of biomacromolecules. This may be due to difficulties such as slow photoactivation kinetics, heat-induced or material surface-induced enzyme instability, or insufficient protein substitution to generate biological responses. It would be highly beneficial if there were a platform for enzymes to be triggered remotely by NIR. Here, as a proof of concept, we use a caged protein kinase A catalytic subunit (PKA) to complex with UCNP to study the feasibility of NIR-triggered enzyme activation and the extent of temporal and spatial resolution in a cellular experiment. PKA is a rapidly reacting signal transduction kinase controlling glycogen synthesis and cytoskeletal regulation that responds to external stimuli *via* cAMP regulation in cytosol.[46−51] Scheme 1 illustrates the design of the caged enzyme−UCNP complex. PKA that was reacted with 2-nitrobenzyl bromide was electrostatically immobilized onto the nanoparticles. NIR irradiation of the UCNPs generated the upconverted UV light, and consequently cleaved the *o*-nitrobenzyl groups and activated PKA.

RESULTS AND DISCUSSION

The detailed synthetic procedure to generate caged PKA/UCNP (and native PKA/UCNP complex) and the characterization of the products are presented in the Materials and Methods section. Negative TEM staining of the silica-coated UCNP and caged PKA/UCNP samples showed protein immobilization (Figure 1).

Caged PKA was immobilized on the $NaYF_4$:Yb^{3+}/Tm^{3+}@SiO_2 (UCNP) surface to utilize the limited amount of upconverted light because the emission intensity is inversely proportional to the distance from the particle squared. The core of caged PKA/UCNP, upon NIR irradiation, emitted upconverted UV light

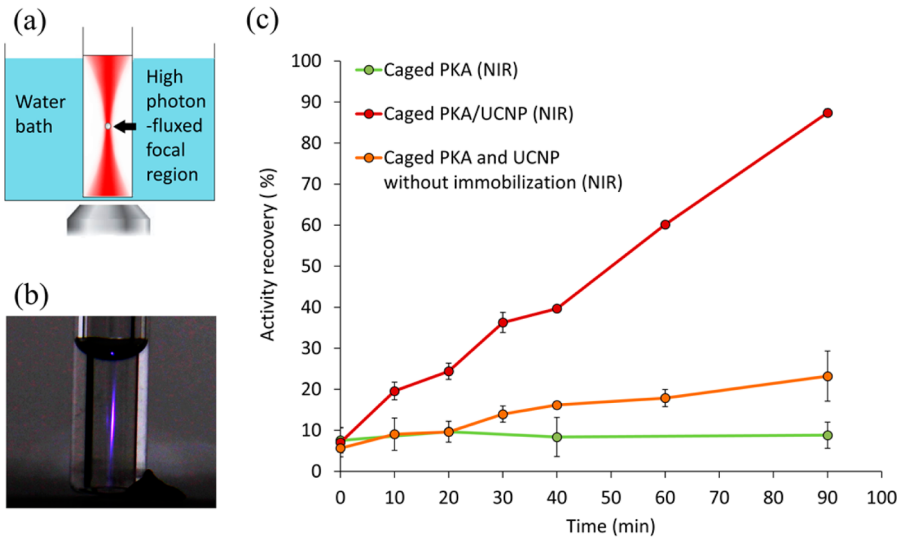

Figure 2. (a) Illustration of the high photon density region focused using an objective lens. (b) The caged PKA/UCNP solution was uncaged with an NIR laser that was focused using a 4× objective lens (uncaging only occurs in the bright purple region). (c) *In vitro* photoactivation of (i) caged PKA/UCNP irradiated by NIR (red), (ii) NIR irradiation of caged PKA without UCNP (green), and (iii) NIR irradiation of caged PKA mixed with PEGylated UCNP, which prevents protein immobilization on the particle surface (orange). To compare the specific activity of the uncaged PKA/UCNP with another important benchmark, free PKA in solution, the values on the *y*-axis of panel c can be converted to the percentage of specific activity of free PKA by multiplying by a factor of 0.6.

(360 nm) from the Tm^{3+}-doped UCNP core (Figure S4, Supporting Information) and photolytically removed the *o*-nitrobenzyl photoprotecting group on caged PKA, thus restoring the kinase activity. The caged PKA/UCNP complex was initially assayed with the irradiation of UV light to make sure that the complex was photoactivatable. The PKA activity was determined by the rate of decrease in NADH absorbance at 340 nm as a function of time after the addition of PKA into the assay mixture. From the slope of the OD *vs* time, the activity of PKA was calculated. The specific activity of caged PKA/UCNP quickly increased over 10-folds and was restored to ~100% relative to a fully UV-uncaged solution of PKA (Figure S8, Supporting Information). During the course of the reaction, the monitoring of PKA activity at 340 nm was not affected by the presence of UCNP (Figure S9, Supporting Information).

The NIR activation of caged PKA/UCNP was assayed and benchmarked against the specific activity of the fully UV-uncaged PKA solution. The caged PKA/UCNP solution was loaded into a flat-ended test tube and irradiated with NIR light. The NIR focal point was adjusted to the center of the solution (Figure 2a). The upconverted UV emission (360 nm) of the caged PKA/UCNP solution (and hence the uncaging process) only occurred in the focal region (Figure 2b) where the photon density was high enough for upconversion due to the nonlinear optical properties of this multiphoton process. This setup slowed the apparent uncaging speed (red curve in Figure 2c) due to the small available uncaging space compared to the total sample volume. We expect that the irradiation time required will be shortened drastically when NIR photolysis is performed in a cellular experiment, where the focal space of the NIR beam is bigger than the intracellular space (*vide infra*). Caged PKA without any UCNP was also irradiated with NIR as a negative control, and it exhibited no activity recovery as expected (green curve in Figure 2c). The NIR-triggered caged PKA in the presence of a PEG3000-grafted UCNP (to prevent PKA nonspecific binding onto the particle surface) recovered only 10% of the kinase activity (orange curve in Figure 2c) compared to the residual activity of the solution of caged PKA. This result suggests that the upconversion-assisted uncaging requires the caged effectors and UCNP to be in close proximity.

Having successfully uncaged the PKA in the test tube, we investigated the feasibility of NIR-induced PKA activation in cells, which would disintegrate the stress fibers. Stress fibers consist of 10−30 strands of filamentous actin (F-actin) that interface with focal adhesions, the cytoskeleton, and the extracellular matrix to maintain the cellular morphology. Stress fibers can be unbundled and disintegrated *via* intracellular PKA activation.[14,52−54] Fluorophore-labeled phalloidin, which strongly binds F-actin, yields a higher staining signal when the stress fibers are disintegrated or unbundled into F-actin filaments.

In a typical cellular experiment, REF52 rat embryonic fibroblast cells were microinjected with caged PKA/UCNP complex, and they were subjected to NIR irradiation, allowing the cells to recover and generate a cellular response for 1 h. These nanoparticles were present in the cytosol, as evidenced by the confocal image after microinjecting the nanoparticle complex into the cell

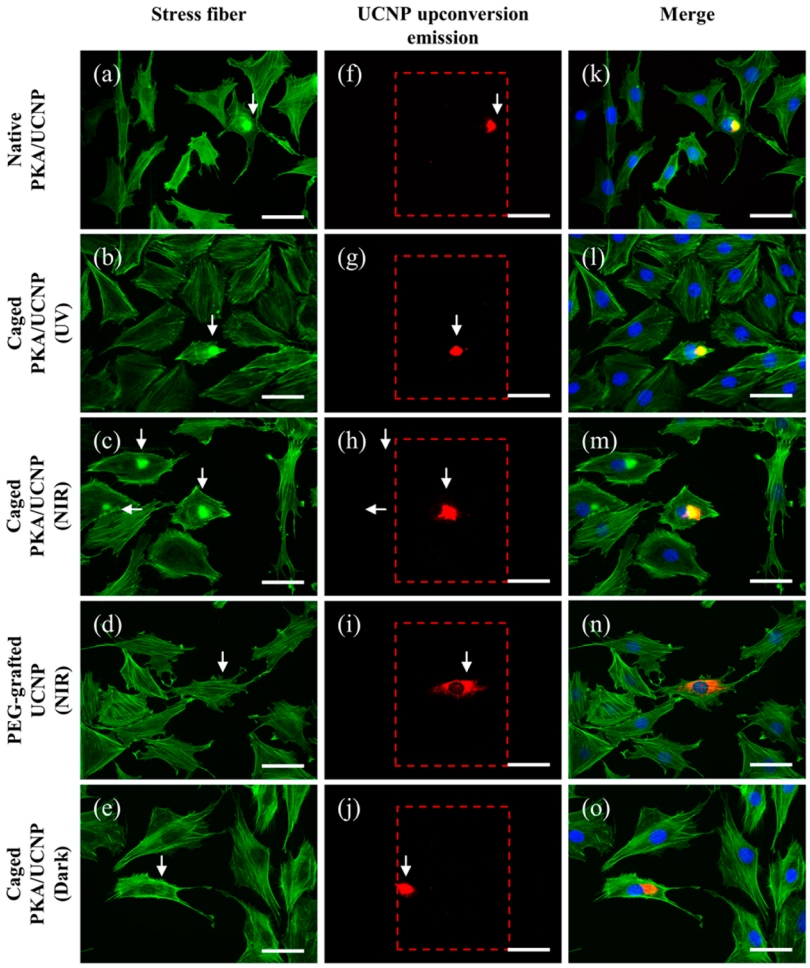

Figure 3. Fluorescence images of REF52 cells microinjected with (a) active PKA/UCNP, (b) caged PKA/UCNP upon UV irradiation, (c) caged PKA/UCNP upon NIR irradiation, (d) PEG-grafted UCNP under NIR irradiation, and (e) caged PKA/UCNP without irradiation. (f–j) The upconverted emission of UCNP (in the dashed box) for (a–e), and (k–o) merged images of the stress fibers, upconversion emissions of the UCNP complex, and DAPI staining of nuclei. For (c, h, and m), NIR photoactivation of the cells, which was using 10× objective lens, generated an illuminating area of 650 × 520 μm^2 (hence, 3 positive cells). When acquiring these fluorescence images, where 40× objective lens was used, the NIR irradiation area was reduced to 150 × 120 μm^2, as shown in the dashed red box (hence, only one cell with upconversion luminescence can be seen). Positive responses for stress fiber disintegration was quantitatively analyzed by ImageJ software. The ratios of the total positive counts and microinjected cells of each experiment were 28/28 in (a), 23/32 in (b), 11/14 in (c), 0/11 in (d), and 0/10 in (e). Unlike the stress fiber disintegration found in the microinjected cells caused by light activated PKA, some of the non-microinjected cells displayed phalloidin staining at cell edges due to the natural filopodial process of cell, which is not related to this experiment. White arrows represent the microinjected cells. Scale bar: 50 μm in all images.

(Figure S10, Supporting Information). The cells were fixed and stained for stress fibers. Figure 3 shows the PKA-triggered downstream effect, disintegration of stress fibers, which is caused by the photoactivation of the caged PKA/UCNP complex. The microinjected cells in the field are shown by white arrows to indicate the effects on the actin cytoskeleton. For positive control experiments, strong stress fiber disintegration was observed using constantly active-PKA/UCNP and UV-activated PKA/UCNP, as shown in Figure 3a,b. The merged images confirm that the active PKA was localized near the particle. The overlap between high phalloidin staining and upconversion luminescence of the particle also implies that the PKA was strongly and stably immobilized on UCNP. For the NIR activation study, REF52 cells were microinjected with the caged PKA/UCNP followed by 980 nm laser irradiation, and these cells exhibited intense phalloidin staining near the particles. This indicates that the stress fiber disintegration was caused by the successful NIR-induced PKA activation, as shown in Figure 3c. As a negative control, the REF52 cells were microinjected with PEG-grafted UCNP (without the caged PKA) followed by NIR irradiation.

The stress fibers were unaffected, which proves that neither the NIR irradiation nor the upconverted UV emission from the UCNP could disintegrate the stress fiber (Figure 3d). In another negative control experiment, which involved injecting REF52 cells with caged PKA/UCNP in the absence of irradiation, no effect on the stress fiber integrity was shown. This result shows that caged PKA/UCNP is enzymatically inert without UV

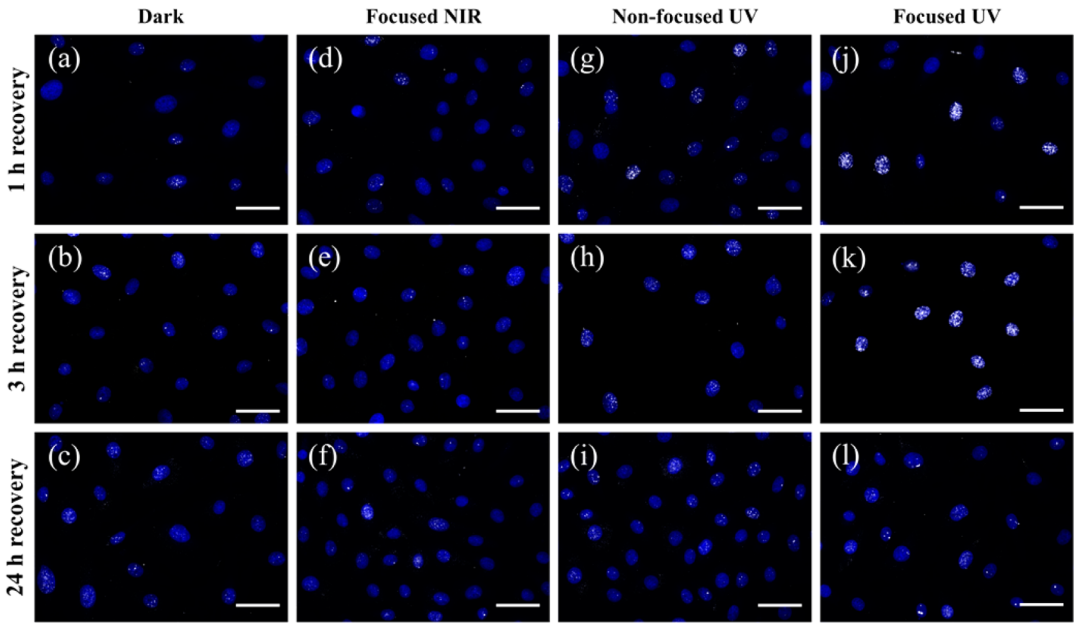

Figure 4. DNA photodamage (histone phosphorylation) caused by UV and NIR exposure was evaluated by anti-phospho-histone H2A.X staining (white spot), and this was overlapped with cell nucleus fluorescence stained by DAPI (purple) after 1, 3, and 24 h recovery. Detailed quantitative analysis are provided in the Figure S16, Supporting Information. REF52 cells show (a−c) control experiment without irradiation, (d−f) focused NIR caused DNA damage level similar to dark-treated cells, and (g and h) nonfocused UV caused DNA damage level after 1 and 3 h recovery, which is slightly higher compared to dark-treated cells. However, in (j and k), significant damage was observed under focused UV irradiation. (i and l) After 24 h recovery, the damage caused by focused UV and nonfocused UV irradiations was not detectable possibly due to the cell self-repair mechanism. Note that the standard deviation of the antibody staining of nonfocused UV was higher than NIR-treated and dark-treated cells (Figure S16, Supporting Information), which indicated that NIR photoactivation approach not only causes less damage, but also provides less statistic uncertainty than the UV photoactivation. Scale bar: 50 μm in all images.

or NIR irradiation, and it indicates that the phalloidin staining was not due to any physical/chemical interactions between phalloidin and the caged PKA/UCNP complex (Figure 3e). Stress fiber disintegration was quantitatively analyzed by ImageJ. The positive response for stress fiber unbundling caused by the PKA particle complex was defined when the staining intensity in the nanoparticle region was over 5 times greater than the background stress fiber staining, as shown in Figure S11, in the Supporting Information. This technique can also be applied to other fibroblastic cells such as NIH-3T3 and MRC-5 cells to disintegrate stress fibers (Figure S15, Supporting Information). To evaluate the extent of DNA damage under light irradiation, cells were photoactivated using different wavelengths of light (nonfocused UV, focused UV and focused NIR), and the DNA damage was quantified by staining with anti-phospho-histone H2A.X (Ser139).[55] The results clearly show that focused UV photoactivation caused significant DNA damage in DNA level within 1 and 3 h recovery (Figure 4j,k). For nonfocused UV photoactivation, although the averaged antibody staining was only slightly higher than the focused NIR, the deviation range was significantly increased (which means a portion of cells was damaged by UV) (Figure S16, Supporting Information). Focused NIR and dark-treated cells have similar average and deviation in staining intensity, which indicating that NIR photoactivation approach is better than UV photoactivation. After 24 h recovery, the damage caused by irradiation was not detectable possibly due to the cell self-repair mechanism (Figure 4c,f,i,l). In addition, to examine the impact of nanoparticles on cellular toxicity over time, the REF52 cells were microinjected with PEG-grafted UCNP, and cellular viability was measured up to 48 h after injection using propidium iodide staining. The results showed no significant cellular toxicity (Figure S17, Supporting Information), indicating that the UCNP platform had no toxicity, as reported in previous publications.[56,57]

To understand the spatiotemporal resolution of this NIR-photoactivation methodology, the cellular responses after NIR irradiation, ranging from second to subseconds, were examined (Figure 5b and Figure S18 in Supporting Information). Strong stress fiber disintegration can still be observed even after 0.1 s of NIR irradiation, indicating excellent temporal resolution of this technique. For spatial resolution (Figure 5c and Figure S19 in Supporting Information), when using a pinhole to control a light spot of subcellular size, PKA can be activated and can cause stress fiber disintegration in a selective fashion.

For more complicated experiments requiring two caged bioeffectors, selective activation cannot be achieved using the conventional UV photoactivation method. Thus, wavelength-selective photoactivation is

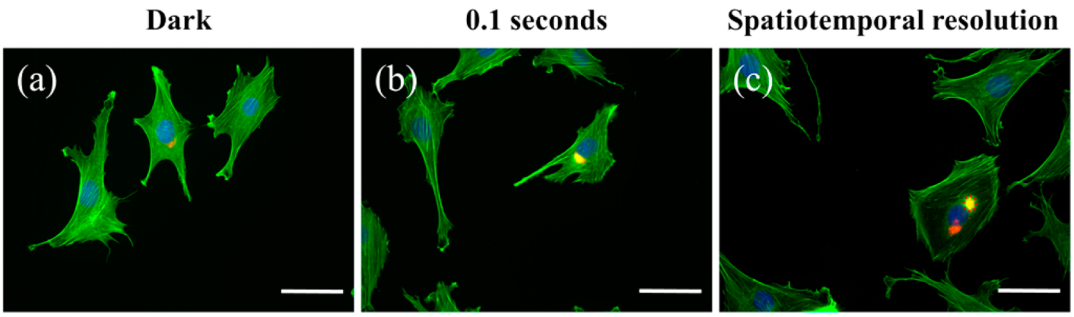

Figure 5. Temporal and spatial resolution of stress fiber disintegration upon NIR irradiation. Fluorescence images of upconversion luminescence (red) and stress fiber staining (green) of REF52 cells that were microinjected with caged PKA/UCNP under (a) dark, (b) NIR irradiation for 0.1 s, and (c) selective subcellular laser spot irradiation (dotted red circle). Scale bar: 50 μm in all images.

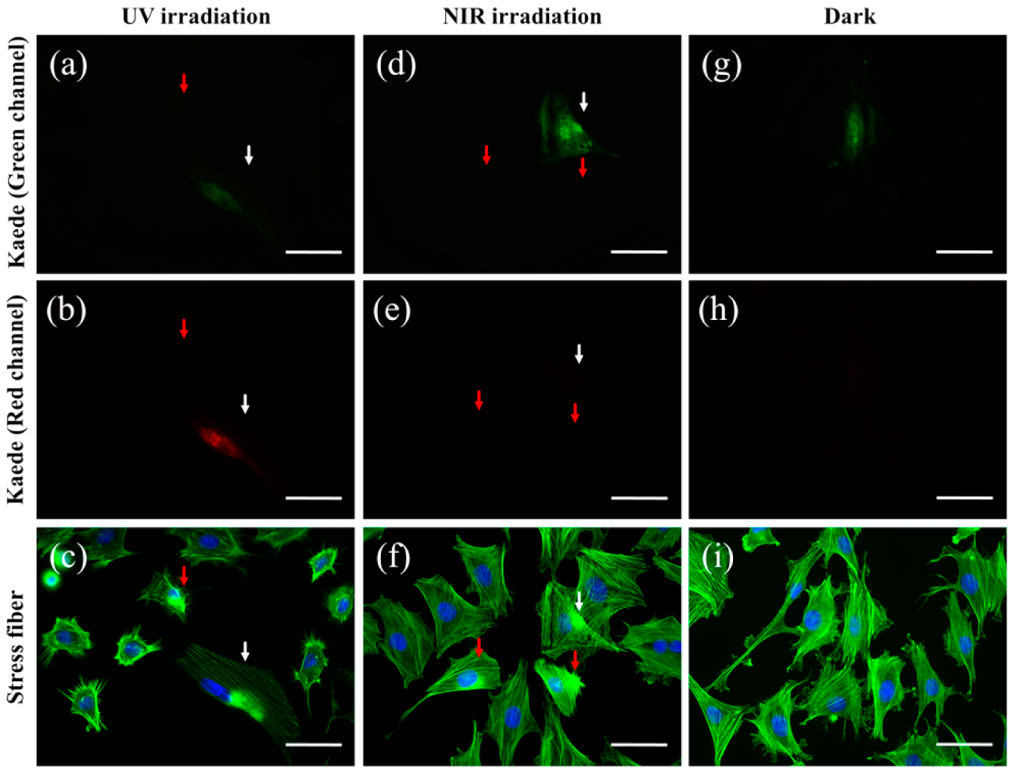

Figure 6. Fluorescence images of REF52 cells. The Kaede-expressing cells under UV irradiation displayed (a) reduced green fluorescence, (b) increased fluorescence in the red channel, and (c) disintegrated stress fibers due to PKA activation. Upon NIR irradiation, the Kaede-expressing cells exhibited (d) no reduction in green fluorescence, (e) unobservable red fluorescence, and (f) stress fiber disintegration due to selective PKA activation. Positive responses for stress fiber disintegration were quantitatively analyzed using ImageJ. The ratios of the total positive counts to microinjected cells in each experiment were 11/13 in (c) and 4/5 in (f). Negative control (dark, without injection) experiments on Kaede-expressing cells showed (g) the original green fluorescence level, (h) original red fluorescence level (which was also unobservable), and (i) no stress fiber disintegration. The white and red arrows indicate the Kaede and non-Kaede expressing cells, respectively, which were microinjected with caged PKA/UCNP. Blue color indicates nuclei stained with DAPI. The bars shown to the right indicate the magnification of the images (50 μm).

also an important technique to be developed for experiments with more than one caged effector. Caging groups that respond to red-shifted light, such as coumarin and cobalamine derivatives, have shown wavelength-selective photoactivation of bioeffectors.[31] In our study, the immobilized caged PKA on the UCNP can be activated by NIR (red curve in Figure 2c). In contrast, we noticed that the nonimmobilized caged PKA mixed with PEG3000-grafted UCNP, which was unable to microscopically approximate the caged PKA, was barely activated with the same upconversion emission intensity upon NIR irradiation (orange curve in Figure 2c). This result implies that the nonimmobilized *o*-nitrobenzyl group caged bioeffectors, even those still sensitive to UV photolysis, may exhibit little or no response to NIR, indicating the possibility of wavelength-selective activation. NIR can be considered to be a separate channel from traditional UV uncaging, in which two caged

effectors have proximity differences to UCNP, even though the uncaging wavelength for the caged PKA and other caged proteins is the same (~360 nm). To prove this hypothesis, Kaede, a green fluorescent protein that can be irreversibly photoconverted from green to red upon UV irradiation, was transfected into the REF52 cells as a second caged protein to test selective photoactivation. The Kaede-expressing cells were then microinjected with caged PKA/UCNP to equip cells with two caged proteins. In conventional UV irradiation, both Kaede and PKA are activated without selectivity, and this is confirmed by showing dim green but strong red fluorescence in Kaede and green color in stress fiber staining, respectively (Figure 6a–c). As expected, NIR irradiation can selectively activate caged PKA/UCNP to disintegrate the stress fibers (Figure 6f) without activating Kaede (strong green and no red fluorescence in Kaede, Figure 6d,e). These results indicate that illuminating at 980 nm can selectively activate the UCNP-immobilized caged protein, whereas the 360 nm light triggers all of the caged proteins. We also noticed that the UV irradiation changed the morphology of some cells due to the phototoxicity of UV (observed in Figure 6c but not Figure 6f), which further emphasizes the importance of this NIR photoactivation technique.

CONCLUSION

In conclusion, we successfully synthesized a caged enzyme/UCNP complex that is triggered by NIR irradiation. The caged PKA/UCNP complex was microinjected into REF52 fibroblast cells and photoactivated using NIR light as an orthogonal messenger. Upon activation, cellular stress fibers were disintegrated. The NIR dosage that we used did not produce observable DNA damage during the cellular experiments, which is a significant advantage compared with conventional UV activation. We also demonstrated that NIR can selectively photoactivate a caged protein (PKA) immobilized on the particle surface while leaving another caged protein (Kaede), which was freely dispersed in the cytosol, inactivate. This important trait of UCNP-assisted photouncaging provides two *de facto* channels for photouncaging experiments. This technique could be potentially generalized to other protein or enzyme classes, and it would be especially useful in light-controlled cellular studies where direct UV exposure is undesirable.

MATERIALS AND METHODS

Materials. All solvents and reagents used for particle synthesis, chromatography, spectroscopy, protein modification, biochemical assays, and photolysis studies were purchased from Sigma-Aldrich and used as received, unless otherwise noted. *Escherichia coli* BL21 (DE3) containing the pET15b plasmid encoding His-tagged cAMP-dependent protein kinase catalytic subunit was obtained from Addgene. Cell culture medium and fetal bovine serum were purchased from Gibco and Biological Industries, respectively. Fluorescence dyes and staining reagents were obtained from Invitrogen. The REF52 cell line was obtained from David Lawrence's group (University of North Carolina at Chapel Hill, Department of Chemistry). The pKaede-MC1 plasmid was purchased from CoralHue.

Instrumentation. X-ray Diffraction (XRD) measurements were performed with a Rigaku XRD DMAX-2200VK diffractometer. TEM images were recorded on a JEOL JEM-1400 120 keV Field Transmission Electron Microscope. The hydrodynamic diameter of the nanoparticles was measured by a Malvern Zetasizer Nano-ZS. Confocal image was obtained using Zeiss LSM 510 META NLO Duoscan. UV–vis, and fluorescence spectral measurements were performed using a Varian Cary 50 spectrophotometer and, a Varian Cary Eclipse fluorescence spectrometer, respectively. Upconversion luminescence was measured using a Varian Cary Eclipse fluorescence spectrometer coupled with a tunable 0.5–8 W 980 nm laser diode (ChangChun New Industry, China) as the excitation source. The 10× Olympus objective lens was installed next to the cuvette holder for the laser to be focused on the middle of the cuvette. Cellular fluorescence and bright field images were obtained by using an Olympus IX-71 fluorescence microscope equipped with a Prior Lumen 200 metal halide light source (directed into the rear port), coupled with a RT3 color CCD system (at the left side port). The customized optical settings for the upconversion channel were set up as follows: A tunable 0.5–8.0 W 980 nm laser diode was installed at the right-side port with the original Olympus IX-71 side port collimator kept (to expand the laser irradiation field after being focused by the objective lens). The filter cube settings for the laser excitation pathway were as follows: emission filter (cutoff is 950 nm; long pass), dichroic mirror (cutoff is 850 nm; short-pass) and emission filter (cutoff is 842 nm; short-pass). All fluorescent images were collected using the same settings, and the corresponding fluorescence staining intensities were quantitatively analyzed using ImageJ software version 1.43n.

In vitro UV photolysis experiments were performed on a UVATA UPS412 system with a UPH-056-365 nm LED. UV and NIR photolysis experiments were also performed on Olympus IX-71 with a metal halide or 980 nm laser light source, respectively. All power densities were measured before (NIR transparent) objective lens focusing using an OPHIR 12A-V1-ROHS thermal pile sensor. Microinjection was performed using a Picospritzer III Microinjection Dispense Systems device coupled with a Narishige MN151/MMO-220A one-axis hydraulic micromanipulator. The original pressure gauge of Picospritzer III was replaced by a ManoMeter PM9100 digital pressure gauge to monitor the pressure in the operating range (approximately 50–200 hPa), and the dispenser valve was sealed in a customized pressuring chamber (15 hPa) to provide compensation pressure for microinjection. Needle was pulled using a Narishige PC-10 puller.

Synthesis of the UCNP Core (β-$NaYF_4$:1.0% Tm^{3+}/30% Yb^{3+}). $Y(CH_3CO_2)_3$ hydrate (99.9%, 0.4527 g, 1.38 mmol), $Yb(CH_3CO_2)_3$ hydrate (99.9%, 0.2533 g, 0.60 mmol) and $Tm(CH_3CO_2)_3$ hydrate (99.9%, 0.0168 g, 0.02 mmol) were added to a 500 mL three-neck round-bottom flask containing octadecene (30 mL) and oleic acid (12 mL). The solution was stirred and heated to 115 °C under vacuum for 30 min to remove residual water and oxygen. The temperature was then lowered to 50 °C under a gentle flow of nitrogen gas. A solution of ammonium fluoride (0.2964 g, 8 mmol) and sodium hydroxide (0.2 g, 5.0 mmol) dissolved in methanol (20 mL) was prepared *via* sonication and then added to the reaction flask at 50 °C. The reaction temperature was then increased to 75 °C followed by increasing the nitrogen flow to remove the methanol from the reaction mixture. The reaction temperature was then increased to 300 °C for 60 min under gentle nitrogen gas flow, and the reaction was allowed to cool to room temperature. The nanoparticles were precipitated by adding ethanol, and they were isolated *via* centrifugation at 8000 g. The resulting pellet was dispersed in a minimal amount of hexanes and precipitated again with excess ethanol. The nanoparticles were then dispersed in cyclohexane for a

subsequent SiO_2 shell-coating procedure. A powder X-ray diffraction (PXRD) study showed that the particle core had a β-hexagonal $NaYF_4$ diffraction pattern (Figure S1, Supporting Information).

Synthesis of Silica-Coated β-$NaYF_4$:1.0%Tm^{3+}/30%Yb^{3+} Core Nanoparticles. A microemulsion method was used to prepare silica-coated β-$NaYF_4$:1.0%Tm^{3+}/30%Yb^{3+}. CO-520 (0.5 mL) and the core nanoparticles (25 mg) were mixed in cyclohexane (10 mL) and stirred for 10 min. Then, ammonia (wt 30%, 0.08 mL) was added, and the container was sonicated for 10 min until a transparent emulsion was formed. Tetraethylorthosilicate (TEOS, 0.04 mL) was then added to the solution, and the solution was stirred for 12 h at room temperature. The silica-coated β-$NaYF_4$ pellets were precipitated by the addition of ethanol and isolated *via* centrifugation at 10 000*g*. The pellets were washed with ethanol/water (1:1, v/v) and then stored in ethanol. Transmission electronic microscopy (TEM) revealed that the UCNP core and silica-coated UCNP sizes were 32 ± 2 and 45 ± 3 nm, respectively (Figure S2, Supporting Information). The dynamic light scattering (DLS) measurements indicated that the silica-coated UCNPs had an average hydrodynamic diameter of 107.3 nm (Figure S3a, Supporting Information). The mean zeta potential of the silica-coated UCNP was ~32.7 mV (Figure S3b, Supporting Information).

Synthesis of PEG3000 Grafted Silica-Coated UCNP. PEG3000, which can prevent nonspecific binding between particle and protein, was used to study the NIR-induced photolysis rate for nonimmobilized caged PKA and UCNP. (3-Mercaptopropyl)trimethoxysilane (MPTMS, 500 μL) was added to the silica-coated nanoparticle (10 mg) solution in dry ethanol (10 mL), and it was stirred for 1 day at 50 °C to couple the free thiol group onto the particle surface. After 1 day, the particles were harvested by centrifugation at 10 000*g* and stored in ethanol. To generate PEG-grafted UCNP, the free thiol group presented on the UCNP (2 mg, 50 nmol of thiol group) was allowed to further react with 300 nmol of the maleimido group of PEG3000-linker, *O*-[*N*-(6-maleimidohexanoyl)aminoethyl]-*O*-[3-(*N*-succinimidyloxy)-3-oxopropyl] polyethylene glycol 3000 (from Sigma-Aldrich) in HEPES pH 7.5 buffer (100 mM) at room temperature. After 1 h, the NHS group was quenched by excess glycine. The PEGylated particles were then washed with water and collected by centrifugation at 17 000*g* for 10 min at 4 °C. They were resuspended in HEPES pH 7.5 buffer (10 mM).

Expression and Purification of PKA and the Synthesis of Caged PKA. *E. coli* BL21 (DE3) containing pET15b plasmid encoding His-tagged cAMP-dependent protein kinase A catalytic subunit was grown in LB medium with 100 μg/mL ampicillin at 37 °C. When the OD_{600} of *E. coli* reached approximately 0.6−0.8, isopropyl β-thiogalactoside (IPTG, 0.4 mM) was applied, and the incubation temperature was changed to 25 °C for 7 h. The *E. coli* cells, after harvest and centrifugation, were then resuspended in the binding buffer (Tris-HCl (20 mM), NaCl (0.5 M), imidazole (5 mM), pH 8.0) and lysed by sonication after the addition of phenylmethanesulfonyl fluoride (PMSF, 0.2 mM). The supernatant of the cell lysate was purified by fast protein liquid chromatography (AKTA FPLC, GE Healthcare) with a HisTrap HP column (5 mL), and PKA was eluted by the same binding buffer with a linear increasing gradient (20−100 mM) of imidazole. The SDS-PAGE analysis is shown in Figure S5, Supporting Information.

After chromatography purification, the PKA eluent was extensively dialyzed against caging buffer, which contains 20 mM Tris-HCl, 100 mM NaCl, and 10 mM $MgCl_2$ at pH 8.5 to remove imidazole, phenylmethylsulfonyl fluoride (PMSF), and dithiothreitol (DTT) prior to the reaction with *o*-nitrobenzyl bromide (NBB). Typically, the caging reaction was performed by incubating 9 μM of PKA with 0.5 mM NBB in caging buffer for 1−2 h at 25 °C. The excess NBB was quenched by 10 mM DTT and then dialyzed against HEPES buffer (10 mM, pH 7.5) to remove excess reagents and salts. The pH was lowered from 8.5 to 7.5 for the subsequent immobilization reaction.

Synthesis of Native PKA/UCNP and Caged PKA/UCNP. To immobilize PKA on silica-coated UCNP *via* electrostatic interactions,[58] PKA (6 nmol) or caged PKA (6 nmol) was incubated with UCNP (1 mg) in HEPES buffer (10 mM, pH 7.5) at 4 °C for 3 h. The mixture was filtrated using PVDF filter (0.45 μm). The particle complex was then centrifuged and redispersed in HEPES (10 mM, pH 7.5) containing 0.1% Prionex (protein stabilizer) to obtain the purified PKA/UCNP complex. After PKA immobilization, the size of the particle was 117.3 nm (Figure S6a, Supporting Information). The zeta potential of the particle complex after PKA immobilization increased from −32.7 to −16.0 mV, which indicated a high level of protein binding (Figure S6b, Supporting Information). The unbounded PKA in supernatant was analyzed by Bradford assay to back-calculate the PKA substitution level on the UCNP particles, which normally have a substitution level of ~4.5 nmol of PKA per mg of particle. Bradford staining experiments showed a strong purple color on the particles, which also suggested a high level and stable protein immobilization without desorption (Figure S7, Supporting Information). The activity of PKA/UCNP also matched the results of the Bradford assay.

PKA Activity Assay. Phosphorylation of the peptide was coupled to pyruvate kinase and lactate dehydrogenase, resulting in the oxidation of NADH. Formation of the latter was monitored by measuring the absorbance decrease of NADH at 340 nm. The activity of PKA was determined in a 60 μL total volume of assay mixture containing 4-morpholinepropanesulfonic acid (MOPS, 100 mM), KCl (100 mM), phosphoenolpyruvate (PEP, 1 mM), ATP (1 mM), NADH (0.8 mM), $MgCl_2$ (1 mM), kemptide (0.4 mM) and a pyruvate kinase/lactate dehydrogenase mixture (30/40 units of PK/LDH). The decrease in NADH absorbance over time was measured after the addition of PKA solution (2 μL) to the assay mixture. The slope of the line directly reflects the activity of the kinase being measured. The immobilization level and specific activity of PKA on the particles are listed in Table S1, Supporting Information.

***In Vitro* UV Photolysis of Caged PKA/UCNP.** Photolysis of caged PKA/UCNP (20 μL, 0.5 mg/mL) solution using UV was performed in a 300 μL flat-end test tube containing uncaging buffer (10 mM HEPES, 5 mM DTT and 1% of Prionex at pH 7.5). The output of the UV LED lamp (UPH-056-365 nm) light source was set to 200 mW/cm^2. Samples were kept in an ice water bath and irradiated for specified durations. After irradiation, PKA activity was measured (Figure S9, Supporting Information).

***In Vitro* NIR Photolysis of Caged PKA/UCNP.** Photolysis of caged PKA/UCNP (20 μL, 0.5 mg/mL) solution and caged PKA + PEG3000-grafted UCNP using NIR were performed in a 300 μL flat-end test tube containing uncaging buffer (10 mM HEPES, 5 mM DTT and 1% of Prionex at pH 7.5). Samples test tube was kept in an ice water bath on Olympus IX-71 stage and irradiated using a 980 nm laser. The power density output was 5 W/cm^2 before 4× objective lens focusing. Samples were irradiated with a 4× objective lens-focused NIR beam for specified durations (10−90 min, where there was a 1 min dark interval for every 10 min irradiation for cooling). After irradiation, the samples were aliquoted for testing PKA activity. Note that the actual uncaging only occurred in the focal point, and the volume was very small.

Microinjection of PKA/UCNP Complexes. Cells were incubated in 10% FBS containing L-15 medium during the microinjection period for stable pH control outside the incubator. Native PKA/UCNP, caged PKA/UCNP or PEGylated UCNP (7.5 mg/mL) were co-injected with 5(6)-carboxytetramethylrhodamine (TAMRA) or 5(6)-carboxyfluorescein (FL) (10 μM) to confirm microinjection completion. Samples were prefiltered through a 0.45 μm filter before needle loading. The concentration of PKA/UCNP particles was chosen to obtain, after microinjection, a cytosolic concentration of PKA (or caged PKA) of 1−3 μM, which is a physiological concentration range for PKA in a cell. Injection pressure was maintained between 50 and 75 hPa with an injection time of 200−300 ms, and the compensation pressure was maintained at 15 hPa. The tip openings of the needles were examined to have an external diameter between 1.3 and 1.5 μm. After microinjection, the cells were subsequently washed with 2 mL of 10% FBS containing L-15 medium.

Photoactivation of Caged PKA/UCNP Using UV or NIR in Living Cells. For UV photoactivation, cells were illuminated on the microscope stage and irradiated by the excitation light filtered by the OLYMPUS U-MWU2 cube, which has a power density of ~15 mW/cm^2, for 3 min without objective lens focusing.

For NIR photoactivation, cells were illuminated on an Olympus IX-71 stage using a 980 nm laser with customized upconversion filter/mirror settings, as described above. The power density output was 5 W/cm^2 before objective lens focusing. Samples were irradiated by NIR focused by a 10× objective lens for 15 min, with a 5 min dark interval after every 5 min irradiation. After UV or NIR photolysis, the cells were allowed to recover at 37 °C for 1 h in complete medium to generate cellular responses, and then subsequently fixed in 4% paraformaldehyde/PBS for 20 min before further staining.

The Spatial and Temporal Resolution of NIR-Activated PKA/UCNP in Living Cells. For the temporal resolution studies of NIR photoactivation (Figure S18, Supporting Information), cells were illuminated as described above, except that the NIR beam was focused by a 40× objective lens (hence, there was greater NIR photon flux, and a shorter irradiation time was needed). Exposure time was controlled using a mechanical shutter positioned in front of the laser (from 0.1 to 1 s). For spatial resolution studies (Figure S19, Supporting Information), the NIR light spot in the view field can be restricted to 4 μm diameter with a pinhole (1 mm in diameter) positioned in front of the laser. After NIR photolysis, the cells were allowed to recover at 37 °C for 1 h in complete medium as previously described to generate cellular responses.

Staining of the Nucleus and DNA Damage. To evaluate the light-induced DNA damage from UV and NIR, if any, we used an anti-phospho-histone H2A.X antibody, a commonly used antibody that can recognize histone phosphorylation due to light-induced DNA damage.[51] The cells were fixed then blocked in 5% FBS, 1% BSA, and 0.1% Tween 20/PBS for 1 h. They were then treated with 1:500 diluted anti-phospho-histone H2A.X (Ser139) (Millipore) in 1% BSA, 0.1% Tween-20/PBS for 1 h. The cells were washed with 0.1% Tween-20/PBS for 5 min 3 times, and then they were incubated with 1:1000 anti-mouse Alexa-594-conjugated secondary antibody in 1% BSA, 0.1% Tween-20/PBS for 1 h to immunofluorescently label the phosphorylated histones produced by DNA damage. The cell nuclei were stained with DAPI (Invitrogen) for 5 min, and stress fibers were stained with Alexa 594-phalloidin (Invitrogen) in PBS for 25 min. After staining, the samples were washed with PBS, and fluorescent images were taken.

Kaede Transfection and Expression. The pKaede-MC1 plasmid was transfected by microinjection to avoid the lipofectamine-induced cell morphological changes. The plasmid was co-injected with 5(6)-carboxytetra-methylrhodamine (10 μM) into REF52 cells with the same microinjection conditions described above and the tip openings of the needles were examined to have an external diameter between 0.7 and 1.0 μm for solution samples. After microinjection, the REF52 cells were incubated for 24 h to screen the Kaede expressing cells and to evaluate the Kaede expression level.

Photoactivation of Cells Containing Both Caged PKA/UCNP and Kaede. Caged PKA/UCNP (7.5 mg/mL) was microinjected into Kaede-expressing cells. After microinjection, the cells were subsequently washed with 2 mL of 10% FBS containing L-15 medium. For NIR photoactivation of cells containing both Kaede and caged PKA/UCNP, cells were illuminated on a microscope stage using a 980 nm laser. The output power density of NIR laser was set to 5 W/cm^2. Samples were irradiated with a NIR beam focused by a 10× objective lens for 15 min total, with a 5 min dark period after every 5 min irradiation. For UV photoactivation, the excitation light, after being filtered by a U-MWU2 cube, had a power density of ~15 mW/cm^2 before objective lens focusing. Cells were irradiated for 30 s with the UV beam focused by a 20× objective lens (estimated power density = 1.5 W/cm^2). After photoactivation, cells were allowed to recover at 37 °C for 1 h in complete medium to develop a cellular response, and they were subsequently fixed in 4% paraformaldehyde/PBS for 20 min for staining/visualization. After fixation, Kaede was visualized using two filter sets (green channel, U-MWB2; red channel, U-MWG2) with a color CCD to confirm the color change. If cellular Kaede was still fluorescing green, we then used Alexa 594-phalloidin to stain and visualize the stress fibers; if cellular Kaede fluorescence changed to red, we switched to Alexa 488-phalloidin to stain and visualize the stress fibers, so that the stress fibers and Kaede could be visualized in different channels without cross interference. Cells were then stained with DAPI (Invitrogen) for 5 min. After staining, the samples were washed with PBS, and fluorescent images of stress fibers and nuclei were taken separately.

Conflict of Interest: The authors declare no competing financial interest.

Supporting Information Available: TEM images and size distribution of silica-coated UCNP and caged PKA/UCNP. The kinase specific activity recovery of caged PKA/UCNP upon UV irradiation. Absorption spectra of caged PKA/UCNP. Fluorescence images of REF52, MRC-5, and NIH/3T3 cells microinjected with caged PKA/UCNP followed by UV or NIR irradiation. Fluorescence images of REF52 cells microinjected with caged PKA/UCNP followed for 0.1 to 1 s, with spatial control of NIR irradiation. Confocal image for the internalization of nanoparticles in cells. Quantitative analysis and statistical data for stress fiber disintegration and DNA damage. The Supporting Information is available free of charge on the ACS Publications website at DOI: 10.1021/acsnano.5b01573.

Acknowledgment. We thank the Nano Science and Technology Program of Academia Sinica and the Ministry of Science and Technology of Taiwan for funding (101-2113-M-001-001-MY2; 103-2113-M-001-028-MY2).

REFERENCES AND NOTES

1. Mayer, G.; Heckel, A. Biologically Active Molecules with a "Light Switch". *Angew. Chem., Int. Ed.* **2006**, *45*, 4900–4921.
2. Priestman, M. A.; Lawrence, D. S. Light-mediated Remote Control of Signaling Pathways. *Biochim. Biophys. Acta, Proteins Proteomics* **2010**, *1804*, 547–558.
3. Shao, Q.; Xing, B. G. Photoactive Molecules for Applications in Molecular Imaging and Cell Biology. *Chem. Soc. Rev.* **2010**, *39*, 2835–2846.
4. Yu, H. T.; Li, J. B.; Wu, D. D.; Qiu, Z. J.; Zhang, Y. Chemistry and Biological Applications of Photo-Labile Organic Molecules. *Chem. Soc. Rev.* **2010**, *39*, 464–473.
5. Brieke, C.; Rohrbach, F.; Gottschalk, A.; Mayer, G.; Heckel, A. Light-Controlled Tools. *Angew. Chem., Int. Ed.* **2012**, *51*, 8446–8476.
6. Klan, P.; Solomek, T.; Bochet, C. G.; Blanc, A.; Givens, R.; Rubina, M.; Popik, V.; Kostikov, A.; Wirz, J. Photoremovable Protecting Groups in Chemistry and Biology: Reaction Mechanisms and Efficacy. *Chem. Rev.* **2013**, *113*, 119–191.
7. Lee, H. M.; Larson, D. R.; Lawrence, D. S. Illuminating the Chemistry of Life: Design, Synthesis, and Applications of "Caged" and Related Photoresponsive Compounds. *ACS Chem. Biol.* **2009**, *4*, 409–427.
8. Goguen, B. N.; Imperiali, B. Chemical Tools for Studying Directed Cell Migration. *ACS Chem. Biol.* **2011**, *6*, 1164–1174.
9. Georgianna, W. E.; Lusic, H.; McLver, A. L.; Deiters, A. Photocleavable Polyethylene Glycol for the Light-Regulation of Protein Function. *Bioconjugate Chem.* **2010**, *21*, 1404–1407.
10. Casey, J. P.; Blidner, R. A.; Monroe, W. T. Caged siRNAs for Spatio-Temporal Control of Gene Silencing. *Mol. Pharmaceutics* **2009**, *6*, 669–685.
11. Riggsbee, C. W.; Deiters, A. Recent Advances in the Photochemical Control of Protein Function. *Trends Biotechnol.* **2010**, *28*, 468–475.
12. Chou, C. J.; Deiters, A. Light-Activated Gene Editing with a Photocaged Zinc-Finger Nuclease. *Angew. Chem., Int. Ed.* **2011**, *50*, 6839–6842.
13. Gautier, A.; Deiters, A.; Chin, J. W. Light-Activated Kinases Enable Temporal Dissection of Signaling Networks in Living Cells. *J. Am. Chem. Soc.* **2011**, *133*, 2124–2127.
14. Lee, H. M.; Xu, W. C.; Lawrence, D. S. Construction of a Photoactivatable Profluorescent Enzyme *via* Propinquity Labeling. *J. Am. Chem. Soc.* **2011**, *133*, 2331–2333.
15. Priestman, M. A.; Sun, L. A.; Lawrence, D. S. Dual Wavelength Photoactivation of cAMP- and cGMP-Dependent Protein Kinase Signaling Pathways. *ACS Chem. Biol.* **2011**, *6*, 377–384.

16. Ui, M.; Tanaka, Y.; Araki, Y.; Wada, T.; Takei, T.; Tsumoto, K.; Endo, S.; Kinbara, K. Application of Photoactive Yellow Protein as a Photoresponsive Module for Controlling Hemolytic Activity of staphylococcal α-Hemolysin. *Chem. Commun.* **2012**, *48*, 4737–4739.
17. Hemphill, J.; Chou, C. J.; Chin, J. W.; Deiters, A. Genetically Encoded Light-Activated Transcription for Spatiotemporal Control of Gene Expression and Gene Silencing in Mammalian Cells. *J. Am. Chem. Soc.* **2013**, *135*, 13433–13439.
18. Matsuo, K.; Kioi, Y.; Yasui, R.; Takaoka, Y.; Miki, T.; Fujishima, S.; Hamachi, I. One-step Construction of Caged Carbonic Anhydrase I Using a Ligand-Directed Acyl Imidazole-Based Protein Labeling Method. *Chem. Sci.* **2013**, *4*, 2573–2580.
19. Rohrbach, F.; Schafer, F.; Fichte, M. A. H.; Pfeiffer, F.; Muller, J.; Potzsch, B.; Heckel, A.; Mayer, G. Aptamer-Guided Caging for Selective Masking of Protein Domains. *Angew. Chem., Int. Ed.* **2013**, *52*, 11912–11915.
20. Oparka, K. J.; Murphy, R.; Derrick, P. M.; Prior, D. A. M.; Smith, J. A. C. Modification of the Pressure-probe Technique Permits Controlled Intracellular Microinjection of Fluorescent Probes. *J. Cell Sci.* **1991**, *98*, 539–544.
21. Carroll, D. J., Ed. *Microinjection: Methods and Applications*; Humana Press, Springer Publications: New York, 2009; Vol. 518.
22. Medintz, I. L.; Pons, T.; Delehanty, J. B.; Susumu, K.; Brunel, F. M.; Dawson, P. E.; Mattoussi, H. Intracellular Delivery of Quantum Dot−Protein Cargos Mediated by Cell Penetrating Peptides. *Bioconjugate Chem.* **2008**, *19*, 1785–1795.
23. Pitchiaya, S.; Heinicke, L. A.; Custer, T. C.; Walter, N. G. Single Molecule Fluorescence Approaches Shed Light on Intracellular RNAs. *Chem. Rev.* **2014**, *114*, 3224–3265.
24. Bender, K.; Blattner, C.; Knebel, A.; Iordanov, M.; Herrlich, P.; Rahmsdorf, H. J. UV-Induced Signal Transduction. *J. Photochem. Photobiol., B* **1997**, *37*, 1–17.
25. Zhang, Y. G.; Dong, Z. M.; Nomura, M.; Zhong, S. P.; Chen, N. Y.; Bode, A. M.; Dong, Z. G. Signal Transduction Pathways Involved in Phosphorylation and Activation of p70S6K Following Exposure to UVA Irradiation. *J. Biol. Chem.* **2001**, *276*, 20913–20923.
26. Zhang, Y. G.; Ma, W. Y.; Kaji, A.; Bode, A. M.; Dong, Z. G. Requirement of ATM in UVA-Induced Signaling and Apoptosis. *J. Biol. Chem.* **2002**, *277*, 3124–3131.
27. He, Y. Y.; Huang, J. L.; Chignell, C. F. Delayed and Sustained Activation of Extracellular Signal-Regulated Kinase in Human Keratinocytes by UVA: Implications in Carcinogenesis. *J. Biol. Chem.* **2004**, *279*, 53867–53874.
28. Amatrudo, J. M.; Olson, J. P.; Lur, G.; Chiu, C. Q.; Higley, M. J.; Ellis-Davies, G. C. R. Wavelength-Selective One- and Two-Photon Uncaging of GABA. *ACS Chem. Neurosci.* **2014**, *5*, 64–70.
29. Bort, G.; Gallavardin, T.; Ogden, D.; Dalko, P. I. From One-Photon to Two-Photon Probes: "Caged" Compounds, Actuators, and Photoswitches. *Angew. Chem., Int. Ed.* **2013**, *52*, 4526–4537.
30. Warther, D.; Guga, S.; Specht, A.; Bolze, F.; Nicoud, J.-F.; Mourot, A.; Goeldner, M. Two-Photon Uncaging: New Prospects in Neuroscience and Cellular Biology. *Bioorg. Med. Chem.* **2010**, *18*, 7753–7758.
31. Priestman, M. A.; Shell, T. A.; Sun, L.; Lee, H. M.; Lawrence, D. S. Merging of Confocal and Caging Technologies: Selective Three-Color Communication with Profluorescent Reporters. *Angew. Chem., Int. Ed.* **2012**, *51*, 7684–7687.
32. Carling, C. J.; Nourmohammadian, F.; Boyer, J. C.; Branda, N. R. Remote-Control Photorelease of Caged Compounds Using Near-Infrared Light and Upconverting Nanoparticles. *Angew. Chem., Int. Ed.* **2010**, *49*, 3782–3785.
33. Yang, Y. M.; Shao, Q.; Deng, R. R.; Wang, C.; Teng, X.; Cheng, K.; Cheng, Z.; Huang, L.; Liu, Z.; Liu, X. G.; et al. *In Vitro* and *in Vivo* Uncaging and Bioluminescence Imaging by Using Photocaged Upconversion Nanoparticles. *Angew. Chem., Int. Ed.* **2012**, *51*, 3125–3129.
34. Boyer, J. C.; Carling, C. J.; Chua, S. Y.; Wilson, D.; Johnsen, B.; Baillie, D.; Branda, N. R. Photomodulation of Fluorescent Upconverting Nanoparticle Markers in Live Organisms by Using Molecular Switches. *Chem.—Eur. J.* **2012**, *18*, 3122–3126.
35. Chien, Y. H.; Chou, Y. L.; Wang, S. W.; Hung, S. T.; Liau, M. C.; Chao, Y. J.; Su, C. H.; Yeh, C. S. Near-Infrared Light Photocontrolled Targeting, Bioimaging, and Chemotherapy with Caged Upconversion Nanoparticles *in Vitro* and *in Vivo*. *ACS Nano* **2013**, *7*, 8516–8528.
36. Dai, Y. L.; Kang, X. J.; Yang, D. M.; Li, X. J.; Zhang, X.; Li, C. X.; Hou, Z. Y.; Cheng, Z. Y.; Ma, P. A.; Lin, J. Platinum (IV) Pro-Drug Conjugated $NaYF_4$:Yb^{3+}/Er^{3+} Nanoparticles for Targeted Drug Delivery and Up-Conversion Cell Imaging. *Adv. Healthcare Mater.* **2013**, *2*, 562–567.
37. Min, Y. Z.; Li, J. M.; Liu, F.; Yeow, E. K. L.; Xing, B. G. Near-Infrared Light-Mediated Photoactivation of a Platinum Antitumor Prodrug and Simultaneous Cellular Apoptosis Imaging by Upconversion-Luminescent Nanoparticles. *Angew. Chem., Int. Ed.* **2014**, *53*, 1012–1016.
38. Jayakumar, M. K. G.; Idris, N. M.; Zhang, Y. Remote Activation of Biomolecules in Deep Tissues Using Near-Infrared-to-UV Upconversion Nanotransducers. *Proc. Natl. Acad. Sci. U.S.A.* **2012**, *109*, 8483–8488.
39. Yang, Y. M.; Liu, F.; Liu, X. G.; Xing, B. G. NIR Light Controlled Photorelease of siRNA and Its Targeted Intracellular Delivery Based on Upconversion Nanoparticles. *Nanoscale* **2013**, *5*, 231–238.
40. Yang, Y. M.; Velmurugan, B.; Liu, X. G.; Xing, B. G. NIR Photoresponsive Crosslinked Upconverting Nanocarriers toward Selective Intracellular Drug Release. *Small* **2013**, *9*, 2937–2944.
41. Liu, J. A.; Bu, W. B.; Pan, L. M.; Shi, J. L. NIR-Triggered Anticancer Drug Delivery by Upconverting Nanoparticles with Integrated Azobenzene-Modified Mesoporous Silica. *Angew. Chem., Int. Ed.* **2013**, *52*, 4375–4379.
42. Yan, B.; Boyer, J. C.; Branda, N. R.; Zhao, Y. Near-Infrared Light-Triggered Dissociation of Block Copolymer Micelles Using Upconverting Nanoparticles. *J. Am. Chem. Soc.* **2011**, *133*, 19714–19717.
43. Wu, T. Q.; Barker, M.; Arafeh, K. M.; Boyer, J. C.; Carling, C. J.; Branda, N. R. A UV-Blocking Polymer Shell Prevents One-Photon Photoreactions while Allowing Multi-Photon Processes in Encapsulated Upconverting Nanoparticles. *Angew. Chem., Int. Ed.* **2013**, *52*, 11106–11109.
44. Zhao, L. Z.; Peng, J. J.; Huang, Q.; Li, C. Y.; Chen, M.; Sun, Y.; Lin, Q. N.; Zhu, L. Y.; Li, F. Y. Near-Infrared Photoregulated Drug Release in Living Tumor Tissue *via* Yolk-Shell Upconversion Nanocages. *Adv. Funct. Mater.* **2014**, *24*, 363–371.
45. Zhou, L.; Chen, Z. W.; Dong, K.; Yin, M. L.; Ren, J. S.; Qu, X. G. DNA-mediated Construction of Hollow Upconversion Nanoparticles for Protein Harvesting and Near-Infrared Light Triggered Release. *Adv. Mater.* **2014**, *26*, 2424–2430.
46. Gibson, R. M.; Ying, J. B.; Taylor, S. S. Identification of Electrostatic Interaction Sites Between the Regulatory and Catalytic Subunits of Cyclic AMP-dependent Protein Kinase. *Protein Sci.* **1997**, *6*, 1825–1834.
47. Banky, P.; Huang, L. J. S.; Taylor, S. S. Dimerization/Docking Domain of the Type Iα Regulatory Subunit of cAMP-dependent Protein Kinase: Requirements for Dimerization and Docking Are Distinct but Overlapping. *J. Biol. Chem.* **1998**, *273*, 35048–35055.
48. Huang, L. J. S.; Taylor, S. S. Dissecting cAMP Binding Domain A in the RIα Subunit of cAMP-dependent Protein Kinase: Distinct Subsites for Recognition of cAMP and the Catalytic Subunit. *J. Biol. Chem.* **1998**, *273*, 26739–26746.
49. Smith, C. M.; Radzio-Andzelm, E.; Madhusudan; Akamine, P.; Taylor, S. S. The Catalytic Subunit of cAMP-dependent Protein Kinase: Prototype for an Extended Network of Communication. *Prog. Biophys. Mol. Biol.* **1999**, *71*, 313–341.
50. Kim, C.; Xuong, N. H.; Taylor, S. S. Crystal Structure of a Complex between the Catalytic and Regulatory (RIα) Subunits of PKA. *Science* **2005**, *307*, 690–696.
51. Kim, C.; Cheng, C. Y.; Saldanha, S. A.; Taylor, S. S. PKA-I Holoenzyme Structure Reveals a Mechanism for cAMP-dependent Activation. *Cell* **2007**, *130*, 1032–1043.

52. Mcclung, J. K.; Kletzien, R. F. Analysis of BHK Cell Growth Kinetics after Microinjection of Catalytic Subunit of Cyclic AMP-dependent Protein Kinase. *Mol. Cell. Biol.* **1984**, *4*, 1079–1085.
53. Roger, P. P.; Rickaert, F.; Huez, G.; Authelet, M.; Hofmann, F.; Dumont, J. E. Microinjection of Catalytic Subunit of Cyclic AMP-Dependent Protein Kinase Triggers Acute Morphological Changes in Thyroid Epithelial Cells. *FEBS Lett.* **1988**, *232*, 409–413.
54. Curley, K.; Lawrence, D. S. Photoactivation of a Signal Transduction Pathway in Living Cells. *J. Am. Chem. Soc.* **1998**, *120*, 8573–8574.
55. Meier, A.; Fiegler, H. Spreading of Mammalian DNA-damage Response Factors Studied By ChIP-chip at Damaged Telomeres. *EMBO J.* **2007**, *26*, 2707–2718.
56. Larson, D. R.; Zipfel, W. R.; Williams, R. M.; Clark, S. W.; Bruchez, M. P.; Wise, F. W.; Webb, W. W. Water-Soluble Quantum Dots for Multiphoton Fluorescence Imaging *in Vivo*. *Science* **2003**, *300*, 1434–1436.
57. Gao, G.; Zhang, C.; Zhou, Z.; Zhang, X.; Ma, J.; Li, C.; Jin, W.; Cui, D. One-pot Hydrothermal Synthesis of Lanthanide Ions Doped One-Dimensional Upconversion Submicrocrystals and Their Potential Application *in Vivo* CT Imaging. *Nanoscale* **2013**, *5*, 351–362.
58. Bolivar, J. M.; Nidetzky, B. Positively Charged Mini-protein Zbasic2 As a Highly Efficient Silica Binding Module: Opportunities for Enzyme Immobilization on Unmodified Silica Supports. *Langmuir* **2012**, *28*, 10040–10049.